Particle and salinity sensing for the marine environment via deep learning using a Raspberry Pi

James A. Grant-Jacob[1], Yunhui Xie[1], Benita S. Mackay[1], Matthew Praeger[1], Michael D. T. McDonnell[1], Daniel J. Heath[1], Matthew Loxham[2], Robert W. Eason[1] and Ben Mills[1]

1 Optoelectronics Research Centre, University of Southampton, Southampton, UK;
2 Faculty of Medicine, University of Southampton, Southampton, UK;
E-mail: J.A.Grant-Jacob@soton.ac.uk; Tel.: +44-238-059-6975

Abstract. The identification of mixtures of particles in a solution via analysis of scattered light can be a complex task, due to the multiple scattering effects between different sizes and types of particles. Deep learning offers the capability for solving complex problems without the need for a physical understanding of the underlying system, and hence offers an elegant solution. Here, we demonstrate the application of convolutional neural networks for the identification of the concentration of microparticles (silicon dioxide and melamine resin) and the solution salinity, directly from the scattered light. The measurements were carried out in real-time using a Raspberry Pi, light source, camera, and neural network computation, hence demonstrating a portable and low-cost environmental marine sensor.

Keywords: Particle pollution, Deep learning, Raspberry Pi, Plastic, Microparticles

1. Introduction

It is estimated that around 35,000 tons of microplastics are present in the world's oceans [1], with trillions of microbeads entering the marine environment daily in aquatic habitats of the United States alone [2]. These microplastics can arise from products such as cosmetics, toothpaste and face scrubs [3,4], which contain microbeads, but can also be formed from the breakdown of larger plastics already discarded into the sea [5,6]. Microplastics can have a direct negative impact on marine organisms [7,8], and impact other marine life through transfer via the food chain [9,10]. They have been found in fish and bivalve organisms, and have been shown to have negative effects on zooplankton and oysters [11–16]. Table salt from around the world has been found to contain microplastics [17,18], and the sea salt contamination, by plastic itself, has been shown to be an indicator of plastic pollution. Drinking water can also contain microplastics [19], and the potential impact on humans has been discussed [20,21], with specific negative impacts on epithelial inflammation [22] and muscle cell behaviour [23].

Monitoring such particles is necessary to help determine origin and distribution, whilst also providing data for mitigating the effects of plastic pollution [24]. Since microplastics can reach the marine floor, having been found in sediments at depths down to 5000 m [25], and in deposit feeders that ingest sediment [26], it is therefore important to monitor plastics before they reach the marine floor. Such a sensing device must have the capability to identify the different types of microplastics and natural occurring particles, such as sand, in order for accurate monitoring. However, a significant obstacle in monitoring such a global problem is the lack of a reliable portable and low-cost method for characterisation of the pollution particles. Manta nets [27] can be used to collect plastic particulate matter from the marine environment of sizes down to ~ 333 μm, with additional laboratory sieving used to separate out smaller micro particles [28,29], and material characterization carried out subsequently using a range of spectroscopic and imaging techniques [30–34]. Such collection and characterization methods are extremely time-consuming and expensive, and hence alternative methods are required.

A holographic technique that involves analysing the scattered light from particles, has shown the potential for the characterisation of particle contaminants in water [35]. Scattered light from particles is dependent on the illumination wavelength and on the particle parameters, such as shape, size, refractive index and composition [36,37], therefore such parameters can be inferred from analysis of the scattered light in certain cases, via comparison to theoretical calculations. In the case of light scattering from a single homogenous sphere, a full electric field calculation, for example via Mie theory, can be used to produce a simulated scattering pattern.

However, the calculations become rapidly more complex as the number of particles is increased, particularly if the particles are not identical. Crucially, however, the inverse calculation is what is needed, as the particle parameters should be determined directly from the scattering pattern. Although particle monitoring from observation of the scattered light has been demonstrated in [35,38], such methods require simulations and lack the flexibility for identification of non-spherical particles. Ideally, the technique should be able to determine the parameters for many particles simultaneously, whilst also being robust enough to deal with real-world effects such as non-spherical particles, variability in light sources and optics, and variability in the aqueous environment.

Deep learning, which is an approach based on the application of neural networks (NNs) [39–41], has already enabled advances in imaging [42,43] and enabled automated classification of objects in images [44,45], such as label-free cell classification [46], as well as object classification through scattering media [47–49] and through scattering pattern imaging [50,51]. Using NNs to determine particle size and refractive index from their scattering pattern was proposed by [52] and has been subsequently demonstrated experimentally on colloidal spherical particles [53–56], showing that NNs can bypass the need to develop complex modelling [57]. Moreover, the ability to update a NN [58], for example to monitor additional particles without the need to physically change a sensor, makes such an approach particularly desirable, especially when implemented on a micro-computer, such as a Raspberry Pi [59,60].

In our previous work, we were able to use a NN to identify single particles of polystyrene and silicon dioxide on a glass substrate, and we demonstrated the ability to use a NN on a desktop computer for the real-time identification of a range of real-world airborne pollution particles (diesel soot, wood ash and pollen) on a glass substrate, directly from their scattering patterns, with each identification taking less than 50 milliseconds [61]. Others have demonstrated the combination of holography and deep learning, for the retrospective (i.e. not real-time) classification of particles in water, using a Raspberry Pi for data collection and with the neural network instead run on a desktop computer [62]. In this work, we demonstrate a Raspberry Pi-based sensor, which runs a neural network, loaded onto it via Wi-Fi, to run in real-time and classify the concentrations in water of 5 µm silicon dioxide (a type of sand) and 8 µm melamine resin (a type of plastic used for tableware [63], which has also been found in fish [64]) microparticles.

Because water salinity can impact on the health of marine life, and is a commonly used ocean parameter to study the effects of climate change [65], the ability to monitor the salinity without the need for additional electrical conductivity devices would be an extra benefit of using the sensing technique documented in this work. We thus also show that it is possible to determine the salt concentration of the water in which 8 µm melamine resin microparticles are present. In addition, we demonstrate the robustness of the NN, by performing a second set of measurements 20 days after the NN was trained, and after deconstructing and rebuilding the experimental setup, hence proving the potential for portable and low-cost sensing.

1.1. Sample preparation

Silicon dioxide microspheres of size 5 µm ± 100 nm (Sigma Aldrich, Product number 44054) and melamine resin microspheres of size 8 µm ± 200 nm (Sigma Aldrich, Product number 95523), with dimensions measured using a Coulter Multisizer II, were deposited via pipette into deionized water-filled glass cuvettes, each of external size 12.5 mm x 12.5 mm x 45 mm, with an optical interaction length of 10 mm. To mimic seawater, saline samples that were used for NN training were prepared by adding salt (sodium chloride) to deionised water-filled cuvettes in steps of 10 ppt (parts per thousand by mass, where 1 ppt is approximately 1 psu (practical salinity unit) [66]), from 0 ppt up to 100 ppt, and 0.1 ppt of 8 µm-sized melamine resin microparticles was added to all samples. Additional cuvettes of deionized water were filled with different concentrations of mixtures of 5 µm silicon dioxide and 8 µm melamine resin microparticles, to give concentrations in the sample solution (referred to here as actual solids concentration) in the range of 0 to 0.1 ppt, in steps of 0.0125 ppt.

1.2. Experimental setup

The schematic of the experimental setup in figure 1 shows light from a ~ 1 mW laser diode operating at 650 nm that has been focused into the cuvette using a 2.5 cm focal length lens. This produced a spot size of approximately 20 µm by 10 µm inside the cuvette. The scattered light from the microparticles was projected onto a white polyester screen 1.5 cm from the cuvette, and subsequently imaged by a CMOS camera (Raspberry Pi Camera Module, CSI-2, 3280 x 2464 pixels), placed 5 cm away. The total volume of the focal region was therefore considerably larger than the volume of a single sphere, enabling the potential for measuring larger particles from

the same sensor design. The camera was connected to a Raspberry Pi 3 Model B+ computer to allow real-time capturing of scattering patterns, every 50 milliseconds, with an exposure time of 20 milliseconds. The images were then transferred to a desktop computer that had an NVIDIA Titan Xp GPU. One hundred scattering patterns were recorded for each of the samples stated in section 2.1 by interchanging the cuvettes in the setup. Each cuvette was shaken by hand prior to placing in the imaging setup. Once the NN was trained on the GPU, the NN was transferred via Wi-Fi to the Raspberry Pi, where it was subsequently used to conduct real-time measurements on scattering images. Here, the NN outputs corresponded to the microparticle mixture concentration, and in the second part of the work, the salinity of the water. The experiments were carried out at room temperature (22 ºC).

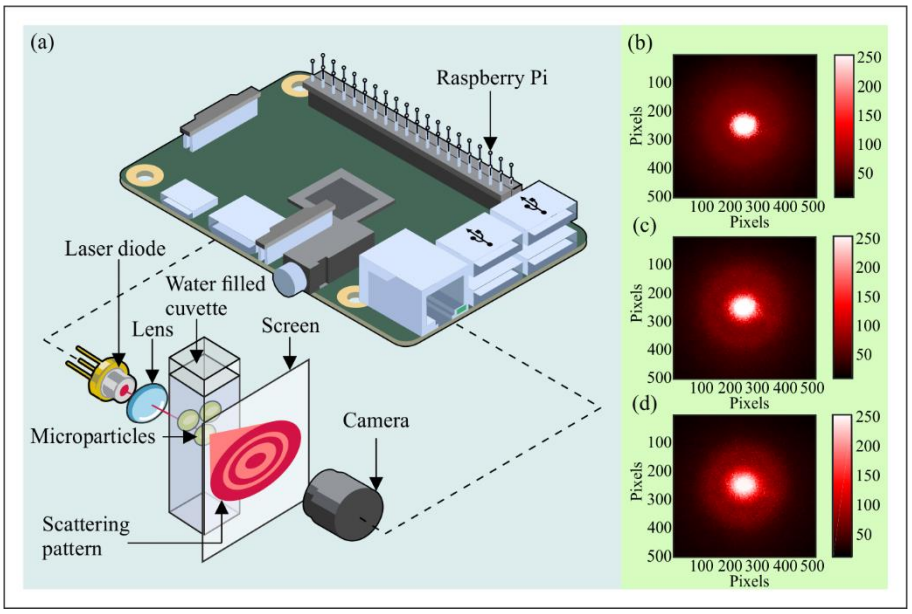

Figure 1. (a) Schematic of setup for sensing microparticles, and salinity, using a Raspberry Pi. Experimentally recorded scattering patterns from (b) 5 µm diameter silicon dioxide microparticles, (c) 8 µm diameter melamine resin microparticles, and (d) mixture of 0.05 ppt 5 µm-sized silicon dioxide microparticles and 0.05 ppt 8 µm-sized melamine resin microparticles.

1.3. Neural network

A convolutional neural network was used, which is a type of NN designed mainly for image processing [57,67], with a regression output. The regression output enabled the capability for the NN to produce a continuous output within a certain range [68]. The NN framework was Tensorflow [69] and was trained on a desktop computer with an NVIDIA Titan Xp graphics processing unit (GPU). Figure 2 shows a schematic of how the NN was used in this work. Owing to the restriction in random-access memory (RAM) that was available for the NN to compute on the Raspberry Pi (1 GB), the input images were cropped such that only one quadrant of the scattering pattern image was selected, in order to still retain high-frequency scattering information in the image data. After cropping, the camera images were resized to 100 x 100 pixels and converted to grayscale. Before the images were sent to the NN, each individual image was normalized to have a mean of 0 and a standard deviation of 1. The NN was formed of two convolutional layers, followed by a max pooling, dropout, and fully connected layer, with a regression output. In the case of the mixture determination, the NN had two outputs, corresponding to the concentration of 5 µm diameter silicon dioxide microparticles and 8 µm diameter melamine resin microparticles. For the salinity measurements, the NN had a single output, corresponding to the ppt of salinity.

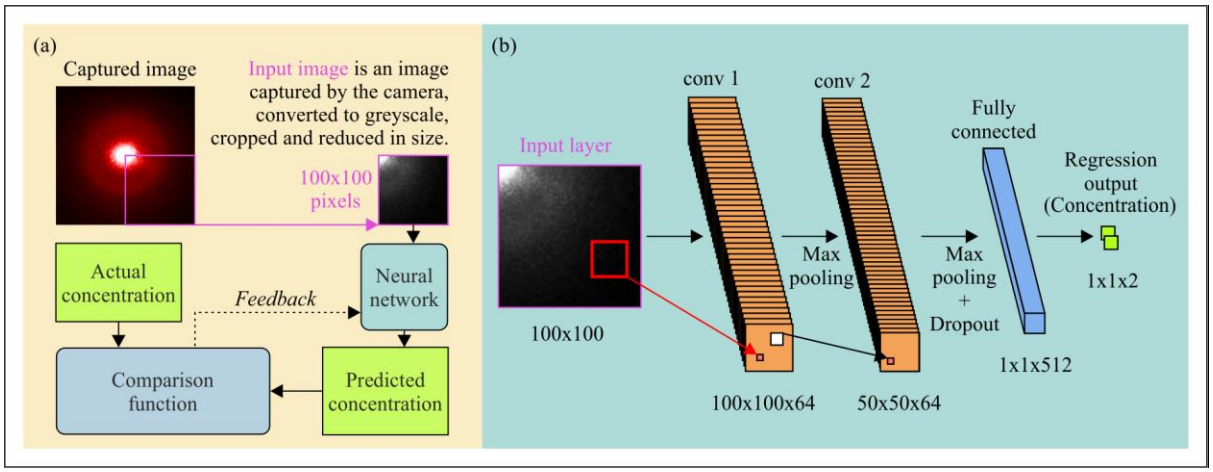

Figure 2. Schematic of the application of the NN for microparticle sensing.

The input layer (greyscale cropped scattering pattern image of 100x100 pixels) was followed by two stages of convolutional then max pooling layers, whereby the convolutional layers had 64 filters with a kernel of 3x3 and stride of 1, and the max pooling layers had a kernel of size 2x2 and stride of 3 [70]. A dropout rate of 50% was used [71], leading to a fully connected layer of 512 neurons and weight decay of 0.0005 [70]. The learning rate of the NNs was 0.0001, while an adaptive moment estimation optimiser [72] was used to minimise mean square error cost function for regression. Through trial and error, the entire architecture was optimised so that the memory requirement of the NN was appropriate to be executed on a Raspberry Pi.

2. Results and discussion

2.1. Identification of microparticle mixture concentration

The NN was designed to produce two numerical outputs from the scattering pattern input, corresponding to the concentration percentage for 5 µm silicon dioxide and 8 µm melamine resin microparticles. The two outputs were independent of each other, and hence could be used to provide absolute concentration values. Figure 3 shows the results for a series of measurements of different mixtures, showing the output for a) 5 µm silicon dioxide and b) 8 µm melamine resin microparticles, where each data point displays the mean and standard deviation for the NN predicted values of the microparticle concentration (predicted solids concentration) from 10 scattering patterns. The NN operated in real-time and entirely on the Raspberry Pi for computation.

One set of test measurements was made on day 1 after the NN was trained, and a second set of test measurements was made 20 days later, following the deconstruction and reconstruction of the experimental setup that occurred after the test measurements on day 1. Whilst the experimental setup was therefore conceptually the same, the exact positioning of the light source, optics, sample and camera was slightly different for the second set of measurements on day 20 (although the cropping window was realigned with the focus of the beam), and hence the fact that the predictive capability of the NN did not decrease illustrates the robustness of this NN approach. The accuracy of the NN could be further improved by increasing the amount of training data, which could be achieved by physically taking more measurements, or artificially, via augmentation [73]. Whilst the particle concentrations in this proof-of-principle demonstration are higher than might be expected in the marine environment [74] owing to the need for sufficient signal collection, our previous work [61] has shown the capability for the identification of single particles using an alternative experimental setup.

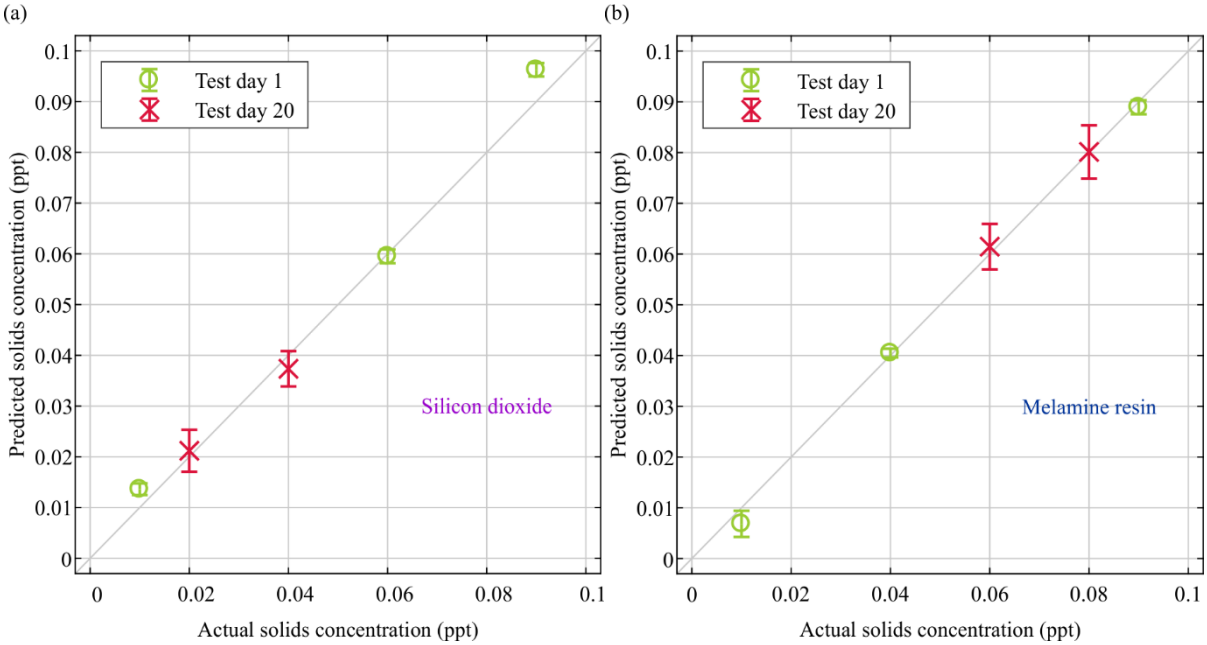

Figure 3. Prediction accuracy for the simultaneous identification of the absolute concentration of a) 5 µm silicon dioxide and b) 8 µm melamine resin microparticles, from a mixture of these particles in a solution. Each data point on the figure, which shows the mean and standard deviation, corresponds to the prediction from 10 scattering patterns. The R-squared value for the silicon dioxide data is 0.9902 and the R-squared value for the melamine resin data is 0.9978.

2.2. Salinity identification

As the concentration of salt in a solution increases from 0 ppt to 100 ppt, a change in the refractive index of the water occurs in which the microparticles are present. For example, at a wavelength of 589.3 nm, the refractive index ranges from 1.334 (0 ppt) to 1.343 (50 ppt) and 1.352 (100 ppt) [75]. Such a change in the refractive index therefore causes a change in the scattering pattern produced by the microparticles. Here, a NN was trained on salinity values of 0 ppt, in steps of 10 ppt, up to 100 ppt, with 10 scattering patterns recorded for each salinity. The NN was then trained for 100 epochs. Subsequently, the NN was trialled on a range of other salinities that corresponded to known values of water bodies, such as the Baltic Sea (8 ppt) and average sea water (35 ppt), which were predicted with mean values and standard deviation of 8.06 ± 1.67 ppt and 34.24 ± 4.03 ppt, respectively (see figure 4). Each data point on the figure corresponds to 10 recorded scattering patterns. The accuracy of the salinity measurements clearly shows the capability of the NN approach for detecting very subtle changes in the scattering patterns.

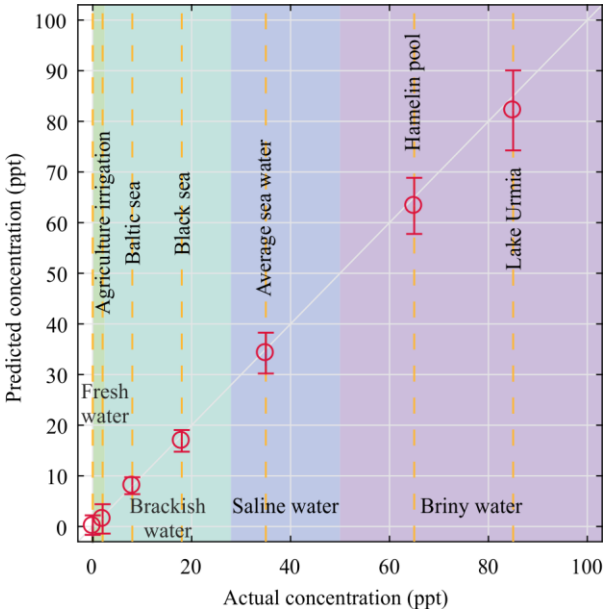

Figure 4. Prediction accuracy of the NN for identification of salinity directly from the scattered light, showing the mean and standard deviation in the prediction. The R-squared value for the data is 0.999. Values of salinity taken from [76–81].

Conclusions

In conclusion, we have shown the simultaneous identification of absolute concentration percentage of 5 μm silicon dioxide and 8 μm melamine resin microparticles, when the particles were present in water. Additionally, we have demonstrated the identification via a NN of salt concentration of water containing 8 μm melamine resin microparticles, for salinities including agriculture irrigation and average sea levels. By running the NN on a Raspberry Pi, we have shown the potential for a portable and low-cost marine environmental sensor. Since the scattering pattern from particles varies depending on the size and material, this proof-of-principle technique, which involves using an NN to classify concentrations of two materials of different sizes and refractive index, could be extended to particles of other sizes and materials, such as polystyrene and polyethylene.

Acknowledgements

BM was supported by an EPSRC Early Career Fellowship (EP/N03368X/1). ML was supported by a BBSRC Future Leader Fellowship (BB/P011365/1) and a NIHR Southampton Biomedical Research Centre Senior Research Fellowship. We gratefully acknowledge the support of NVIDIA Corporation with the donation of the Titan Xp GPU used for this research, donated through NVIDIA GPU Grant Program. Data supporting this submission is available at https://doi.org/10.5258/SOTON/D0758

ORCID iDs

James A Grant-Jacob https://orcid.org/0000-0002-4270-4247

Yunhui Xie https://orcid.org/0000-0002-8841-7235

Benita S Mackay https://orcid.org/0000-0003-2050-8912

Matthew Praeger https://orcid.org/0000-0002-5814-6155

Michael D T McDonnell https://orcid.org/0000-0003-4308-1165

Daniel J Heath https://orcid.org/0000-0003-3566-1813

Matthew Loxham https://orcid.org/0000-0001-6459-538X

Robert W Eason https://orcid.org/0000-0001-9704-2204

Ben Mills https://orcid.org/0000-0002-1784-1012

References

[1] Eriksen M, Lebreton L C M, Carson H S, Thiel M, Moore C J, Borerro J C, Galgani F, Ryan P G and Reisser J 2014 Plastic pollution in the world's oceans: more than 5 trillion plastic pieces weighing over 250,000 tons afloat at sea *PLoS One* **9** e111913

[2] Rochman C M, Kross S M, Armstrong J B, Bogan M T, Darling E S, Green S J, Smyth A R and Veríssimo D 2015 Scientific Evidence Supports a Ban on Microbeads *Environ. Sci. Technol.* **49** 10759–61

[3] Napper I E, Bakir A, Rowland S J and Thompson R C 2015 Characterisation, quantity and sorptive properties of microplastics extracted from cosmetics *Mar. Pollut. Bull.* **99** 178–85

[4] Cheung P K and Fok L 2016 Evidence of microbeads from personal care product contaminating the sea *Mar. Pollut. Bull.* **109** 582–5

[5] Arthur C, Baker J and Bamford H 2009 *Proceedings of the International Research Workshop on the Occurrence, Effects, and Fate of Microplastic Marine Debris, September 9-11, 2008*

[6] Costa M F, Do Sul J A I, Silva-Cavalcanti J S, Araújo M C B, Spengler Â and Tourinho P S 2010 On the importance of size of plastic fragments and pellets on the strandline: a snapshot of a Brazilian beach *Environ. Monit. Assess.* **168** 299–304

[7] Cózar A, Echevarría F, González-Gordillo J I, Irigoien X, Úbeda B, Hernández-León S, Palma Á T, Navarro S, García-de-Lomas J, Ruiz A, Fernández-de-Puelles M L and Duarte C M 2014 Plastic debris in the open ocean *Proc. Natl. Acad. Sci.* **111** 10239–44

[8] Cole M, Lindeque P, Fileman E, Halsband C, Goodhead R, Moger J and Galloway T S 2013 Microplastic ingestion by zooplankton *Environ. Sci. Technol.* **47** 6646–55

[9] Andrady A L 2011 Microplastics in the marine environment *Mar. Pollut. Bull.* **62** 1596–605

[10] Setälä O, Fleming-Lehtinen V and Lehtiniemi M 2014 Ingestion and transfer of microplastics in the planktonic food web *Environ. Pollut.* **185** 77–83

[11] Rummel C D, Löder M G J, Fricke N F, Lang T, Griebeler E-M, Janke M and Gerdts G 2016 Plastic ingestion by pelagic and demersal fish from the North Sea and Baltic Sea *Mar. Pollut. Bull.* **102** 134–41

[12] Tanaka K and Takada H 2016 Microplastic fragments and microbeads in digestive tracts of planktivorous fish from urban coastal waters *Sci. Rep.* **6** 34351

[13] Van Cauwenberghe L, Claessens M, Vandegehuchte M B and Janssen C R 2015 Microplastics are taken up by mussels (Mytilus edulis) and lugworms (Arenicola marina) living in natural habitats *Environ. Pollut.* **199** 10–7

[14] Sussarellu R, Suquet M, Thomas Y, Lambert C, Fabioux C, Eve M and Pernet J 2016 Oyster reproduction is affected by exposure to polystyrene microplastics **113** 2430–5

[15] Lee K-W, Shim W J, Kwon O Y and Kang J-H 2013 Size-dependent effects of micro polystyrene particles in the marine copepod Tigriopus japonicus *Environ. Sci. Technol.* **47** 11278–83

[16] Cole M, Lindeque P, Fileman E, Halsband C and Galloway T S 2015 The impact of polystyrene microplastics on feeding, function and fecundity in the marine copepod Calanus helgolandicus *Environ. Sci. Technol.* **49** 1130–7

[17] Iñiguez M E, Conesa J A and Fullana A 2017 Microplastics in spanish table salt *Sci. Rep.* **7** 8620

[18] Yang D, Shi H, Li L, Li J, Jabeen K and Kolandhasamy P 2015 Microplastic pollution in table salts from China *Environ. Sci. Technol.* **49** 13622–7

[19] Kosuth M, Wattenberg E V, Mason S A, Tyree C and Morrison D 2017 Synthetic polymer contamination in global drinking water *Orb https//orbmedia. org/stories/Invisibles_plastics/multimedia*

[20] Bouwmeester H, Hollman P C H and Peters R J B 2015 Potential health impact of environmentally released micro-and nanoplastics in the human food production chain: experiences from nanotoxicology *Environ. Sci. Technol.* **49** 8932–47

[21] Rist S, Almroth B C, Hartmann N B and Karlsson T M 2018 A critical perspective on early communications concerning human health aspects of microplastics *Sci. Total Environ.* **626** 720–6

[22] Brown D M, Wilson M R, MacNee W, Stone V and Donaldson K 2001 Size-Dependent Proinflammatory Effects of Ultrafine Polystyrene Particles: A Role for Surface Area and Oxidative Stress in the Enhanced Activity of Ultrafines *Toxicol. Appl. Pharmacol.* **175** 191–9

[23] Berntsen P, Park C Y and Tsuda A 2010 Biomechanical effects of environmental and engineered particles on human airway smooth muscle cells

[24] Ryan P G, Moore C J, van Franeker J A and Moloney C L 2009 Monitoring the abundance of plastic debris in the marine environment *Philos. Trans. R. Soc. B Biol. Sci.* **364** 1999–2012

[25] Van Cauwenberghe L, Vanreusel A, Mees J and Janssen C R 2013 Microplastic pollution in deep-sea sediments *Environ. Pollut.* **182** 495–9

[26] Nel H A, Dalu T and Wasserman R J 2018 Sinks and sources: Assessing microplastic abundance in river sediment and deposit feeders in an Austral temperate urban river system *Sci. Total Environ.* **612** 950–6

[27] Reisser J, Shaw J, Wilcox C, Hardesty B D, Proietti M, Thums M and Pattiaratchi C 2013 Marine Plastic Pollution in Waters around Australia: Characteristics, Concentrations, and Pathways *PLoS One* **8** e80466

[28] Claessens M, De Meester S, Van Landuyt L, De Clerck K and Janssen C R 2011 Occurrence and distribution of microplastics in marine sediments along the Belgian coast *Mar. Pollut. Bull.* **62** 2199–204

[29] Lattin G L, Moore C J, Zellers A F, Moore S L and Weisberg S B 2004 A comparison of neustonic plastic and zooplankton at different depths near the southern California shore *Mar. Pollut. Bull.* **49** 291–4

[30] Harrison J P, Ojeda J J and Romero-González M E 2012 The applicability of reflectance micro-Fourier-transform infrared spectroscopy for the detection of synthetic microplastics in marine sediments *Sci. Total Environ.* **416** 455–63

[31] Imhof H K, Ivleva N P, Schmid J, Niessner R and Laforsch C 2013 Contamination of beach sediments of a subalpine lake with microplastic particles *Curr. Biol.* **23** R867--R868

[32] Eriksen M, Mason S, Wilson S, Box C, Zellers A, Edwards W, Farley H and Amato S 2013 Microplastic pollution in the surface waters of the Laurentian Great Lakes *Mar. Pollut. Bull.* **77** 177–82

[33] Faure F, Gagnaux V, Baecher H, Neuhaus V and de Alencastro L 2013 Microplastiques sur les plages et la surface du Léman. Résultats préliminaires *Bull. l" ARPEA* **49** 15–8

[34] Gasperi J, Dris R, Bonin T, Rocher V and Tassin B 2014 Assessment of floating plastic debris in surface water along the Seine River *Environ. Pollut.* **195** 163–6

[35] Philips L A, Ruffner D B, Cheong F C, Blusewicz J M, Kasimbeg P, Waisi B, McCutcheon J R and Grier D G 2017 Holographic characterization of contaminants in water: Differentiation of suspended particles in heterogeneous dispersions *Water Res.* **122** 431–9

[36] Bohren C F and Huffman D R 2008 *Absorption and scattering of light by small particles* (John Wiley & Sons)

[37] Mills B, Chau C F, Rogers E T F, Grant-Jacob J, Stebbings S L, Praeger M, de Paula A M, Froud C A, Chapman R T, Butcher T J, Baumberg J J, Brocklesby W S and Frey J G 2008 Direct measurement of the complex refractive index in the extreme ultraviolet spectral region using diffraction from a nanosphere array *Appl. Phys. Lett.* **93** 231103

[38] Wu Y and Ozcan A 2017 Lensless digital holographic microscopy and its applications in biomedicine and environmental monitoring *Methods* **136** 4–16

[39] Günther J, Pilarski P M, Helfrich G, Shen H and Diepold K 2014 First Steps Towards an Intelligent Laser Welding Architecture Using Deep Neural Networks and Reinforcement Learning *Procedia Technol.* **15** 474–83

[40] Rowley H A, Baluja S and Kanade T 1998 Neural network-based face detection *IEEE Trans. Pattern Anal. Mach. Intell.* **20** 23–38

[41] Hinton G E and Salakhutdinov R R 2006 Reducing the dimensionality of data with neural networks *Sciencemag* **313** 504–7

[42] Rivenson Y, Göröcs Z, Günaydin H, Zhang Y, Wang H and Ozcan A 2017 Deep learning microscopy *Optica* **4** 1437–43

[43] Rivenson Y, Zhang Y, Günaydin H, Teng D and Ozcan A 2018 Phase recovery and holographic image reconstruction using deep learning in neural networks *Light Sci. Appl.* **7** 17141

[44] LeCun Y, Bengio Y and Hinton G 2015 Deep learning *Nature* **521** 436

[45] Mills B, Heath D J, Grant-Jacob J A, Xie Y and Eason R W 2018 Image-based monitoring of femtosecond laser machining via a neural network *J. Phys. Photonics* **1** 15008

[46] Chen C L, Mahjoubfar A, Tai L-C, Blaby I K, Huang A, Niazi K R and Jalali B 2016 Deep Learning in Label-free Cell Classification *Sci. Rep.* **6** 21471

[47] Li S, Deng M, Lee J, Sinha A and Barbastathis G 2017 Imaging through glass diffusers using densely connected convolutional networks *arXiv Prepr. arXiv1711.06810*

[48] Satat G, Tancik M, Gupta O, Heshmat B and Raskar R 2017 Object classification through scattering media with deep learning on time resolved measurement *Opt. Express* **25** 17466–79

[49] Valent E and Silberberg Y 2018 Scatterer recognition via analysis of speckle patterns *Optica* **5** 204–7

[50] Dong K, Feng Y, Jacobs K M, Lu J Q, Brock R S, Yang L V, Bertrand F E, Farwell M A and Hu X-H 2011 Label-free classification of cultured cells through diffraction imaging *Biomed. Opt. Express* **2** 1717–26

[51] Jo Y, Park S, Jung J, Yoon J, Joo H, Kim M, Kang S-J, Choi M C, Lee S Y and Park Y 2017 Holographic deep learning for rapid optical screening of anthrax spores *Sci. Adv.* **3** e1700606

[52] Ulanowski Z, Wang Z, Kaye P H and Ludlow I K 1998 Application of neural networks to the inverse light scattering problem for spheres *Appl. Opt.* **37** 4027–33

[53] Lee S-H, Roichman Y, Yi G-R, Kim S-H, Yang S-M, Van Blaaderen A, Van Oostrum P and Grier D G 2007 Characterizing and tracking single colloidal particles with video holographic microscopy *Opt. Express* **15** 18275–82

[54] Perry R W, Meng G, Dimiduk T G, Fung J and Manoharan V N 2012 Real-space studies of the structure and dynamics of self-assembled colloidal clusters *Faraday Discuss.* **159** 211–34

[55] Wang C, Cheong F C, Ruffner D B, Zhong X, Ward M D and Grier D G 2016 Holographic characterization of colloidal fractal aggregates *Soft Matter* **12** 8774–80

[56] Yevick A, Hannel M and Grier D G 2014 Machine-learning approach to holographic particle characterization *Opt. Express* **22** 26884–90

[57] Mills B, Heath D J, Grant-Jacob J A and Eason R W 2018 Predictive capabilities for laser machining via a neural network *Opt. Express* **26** 17245–53

[58] Achille A, Eccles T, Matthey L, Burgess C P, Watters N, Lerchner A and Higgins I 2018 Life-Long Disentangled Representation Learning with Cross-Domain Latent Homologies *arXiv Prepr. arXiv1808.06508*

[59] Raspberry Pi Foundation 2016 Raspberry Pi 3 Model B *Raspberry Pi Website*

[60] Ferdoush S and Li X 2014 Wireless sensor network system design using Raspberry Pi and Arduino for environmental monitoring applications *Procedia Comput. Sci.* **34** 103–10

[61] Grant-Jacob J A, Mackay B S, Baker J A G, Heath D J, Xie Y, Loxham M, Eason R W and Mills B 2018 Real-time particle pollution sensing using machine learning *Opt. Express* **26** 27237–46

[62] Hannel M D, Abdulali A, O'Brien M and Grier D G 2018 Machine-learning techniques for fast and

accurate feature localization in holograms of colloidal particles *Opt. Express* **26** 15221–31

[63] Powers P O 1953 Phenol-, Urea-, and Melamine-Formaldehyde Plastics *Ind. Eng. Chem.* **45** 1063–6

[64] Nelms S E, Galloway T S, Godley B J, Jarvis D S and Lindeque P K 2018 Investigating microplastic trophic transfer in marine top predators *Environ. Pollut.* **238** 999–1007

[65] Kaidarova A, Marengo M, Marinaro G, Geraldi N, Duarte C M and Kosel J 2018 Flexible and Biofouling Independent Salinity Sensor *Adv. Mater. Interfaces* **5** 1801110

[66] Pawlocwicz P, McDougall T J, Feistel R and Tailleux R 2012 An historical perspective on the development of the thermodynamic equation of seawater-2010 *Ocean Sci.* **8** 161–74

[67] Heath D J, Grant-Jacob J A, Xie Y, Mackay B S, Baker J A G, Eason R W and Mills B 2018 Machine learning for 3D simulated visualization of laser machining *Opt. Express* **26** 4984–8

[68] Specht D F 1991 A general regression neural network *IEEE Trans. neural networks* **2** 568–76

[69] Abadi M, Barham P, Chen J, Chen Z, Davis A, Dean J, Devin M, Ghemawat S, Irving G, Isard M and others 2016 Tensorflow: a system for large-scale machine learning *OSDI* vol 16 pp 265–83

[70] Krizhevsky A, Sutskever I and Hinton G E 2012 Imagenet classification with deep convolutional neural networks *Advances in neural information processing systems* pp 1097–105

[71] Srivastava N, Hinton G, Krizhevsky A, Sutskever I and Salakhutdinov R 2014 Dropout: A simple way to prevent neural networks from overfitting *J. Mach. Learn. Res.* **15** 1929–58

[72] Kingma D P and Ba J 2014 Adam: A method for stochastic optimization *arXiv Prepr. arXiv1412.6980*

[73] Perez L and Wang J 2017 The effectiveness of data augmentation in image classification using deep learning *arXiv Prepr. arXiv1712.04621*

[74] Bergmann M, Wirzberger V, Krumpen T, Lorenz C, Primpke S, Tekman M B and Gerdts G 2017 High Quantities of Microplastic in Arctic Deep-Sea Sediments from the HAUSGARTEN Observatory *Environ. Sci. Technol.* **51** 11000–10

[75] Tan C-Y and Huang Y-X 2015 Dependence of refractive index on concentration and temperature in electrolyte solution, polar solution, nonpolar solution, and protein solution *J. Chem. Eng. Data* **60** 2827–33

[76] Nissling A 1994 Survival of eggs and yolk-sac larvae of Baltic cod (Gadus morhua L.) at low oxygen levels in different salinities *ICES Marine Science Symposia* vol 198 pp 626–31

[77] Mudie P J, Aksu A E and Yasar D 2001 Late Quaternary dinoflagellate cysts from the Black, Marmara and Aegean seas: variations in assemblages, morphology and paleosalinity *Mar. Micropaleontol.* **43** 155–78

[78] Agh N, Abatzopoulos T J, Kappas I, Van Stappen G, Razavi Rouhani S M and Sorgeloos P 2007 Coexistence of Sexual and Parthenogenetic Artemia Populations in Lake Urmia and Neighbouring Lagoons *Int. Rev. Hydrobiol.* **92** 48–60

[79] Burkholder D A, Fourqurean J W and Heithaus M R 2013 Spatial pattern in seagrass stoichiometry indicates both N-limited and P-limited regions of an iconic P-limited subtropical bay *Mar. Ecol. Prog. Ser.* **472** 101–15

[80] Glenn E P, Brown J J and O'Leary J W 1998 Irrigating Crops with Seawater *Sci. Am.* **279** 76–81

[81] Rahman T, Mirza A T M, Rahman S H and Majumder R K 2012 Groundwater quality for irrigation of deep aquifer in southwestern zone of Banglades. *Songklanakarin J. Sci. Technol.* **34**